Dry Sliding Wear and Friction Behavior of Graphene/ZrO$_2$ Binary Nanoparticles Reinforced Aluminum Hybrid Composites

Mahmut Can Şenel[1] · Muzaffer Üstün[1]

Abstract

Recently, aluminum matrix composites have been fabricated by pure zirconia (ZrO$_2$) or pure graphene in the aluminum matrix because of good solid lubricant property of graphene and high compressive strength of ZrO$_2$. Nevertheless, there is no study on the effect of both ZrO$_2$ and graphene reinforced aluminum composite. In this current work, the tribological behaviors of Al-ZrO$_2$ and Al-ZrO$_2$-graphene composites with various contents (ZrO$_2$: 1–12wt.%; graphene: 0.15–0.45wt.%) were investigated under different loads (5 and 10 N) via the pin-on-disk wear test unit. The density, porosity, hardness, and compressive strength were investigated by the Archimedes' principle kit, Vickers hardness test unit, and universal test machine, respectively. According to the test results, the micro-Vickers hardness, porosity, and compressive strength enhanced from 30 ± 1.2 HV, 7%, 186 ± 4 MPa (pure Al) to 75 ± 2 HV, 3.7%, 490 ± 4 MPa (Al-9%ZrO$_2$-0.15%graphene), respectively. Similarly, the lowest friction coefficient (0.18 under a 10 N load), the mass loss (0.011 g under a 5 N load), and wear rate (0.0031 mm^3/(Nm) under a 5 N load) were obtained at the Al-9%ZrO$_2$-0.15%graphene composite. The mechanical strength and tribological behaviors of Al hybrid composites deteriorated in the case of over 9wt.%ZrO$_2$ and 0.15wt.%graphene contents due to the agglomerations of graphene and ZrO$_2$ nanoparticles. Therefore, it may be concluded that graphene is an excellent solid lubricator, and ZrO$_2$ has a remarkable wear resistance for Al hybrid composites.

Keywords Composite · Graphene · Aluminum · ZrO$_2$ · Wear · Friction

1 Introduction

Nowadays, research has continued to get over the monolithic materials' restrictions and produce cost-effective hybrid materials with superior characteristics to meet industrial demands [1]. In the automotive, aerospace, and aircraft industries, aluminum metal matrix composites (AMMCs) are fascinating because of their superior properties like their high elastic modulus, excellent wear resistance, and low density [2–4]. AMMCs have proven to be one of the most promising engineering materials for different reinforcement materials such as silicon nitride (Si$_3$N$_4$) [5], silicon carbide (SiC) [6], boron carbide (B$_4$C) [7], boron nitride (BN) [8], aluminum oxide (Al$_2$O$_3$) [9], titanium carbide (TiC) [10], titanium diboride (TiN) [11], and zirconia (ZrO$_2$) [12].

In recent years, aluminum matrix nanocomposites have been thought to be influential materials due to their excellent properties and multifunctionality [13, 14]. They are a new type of composites comprised of combining one or a few nano-reinforcements' types incorporated into the Al matrix. These composites enable them to utilize the unique superior properties of individual contributing nano-reinforcements [15]. The promising mechanical and tribological properties of Al matrix nanocomposites are significantly contributing to a fast enhancement in their popularity and a considerable widening in their application areas [16, 17]. Compared with the conventional composites, Al hybrid nanocomposites demonstrate excellent properties like the resistance to crack propagation, high strength, and more phenomenal plasticity at extreme loads [18]. Besides, nanocomposites provide an increased variety of designs for the materials' selection to meet the application requirements [19]. The favorable multifunctional properties of nanocomposites are researched in

✉ Mahmut Can Şenel
  mahmutcan.senel@omu.edu.tr

  Muzaffer Üstün
  ustunmuzafferkaan@gmail.com

1 Mechanical Engineering Department, Ondokuz Mayıs University, 55220 Samsun, Turkey

many industrial areas like aerospace, automobile, marine, and aeronautical [20–22].

Recently, graphene nanoplatelets (GNPs) may be used in metal matrix composites as a reinforcement material due to graphene's unusual morphology and bonding structure [23, 24]. The structure of graphene resembles a single layer of graphite. It has a very high melting point and is very strong because of its sizeable regular arrangement of carbon atoms joined by covalent bonds. It has outstanding properties such as high thermal/electrical conductivity, high hardness, and high elasticity modulus. These properties have attracted many researchers for improving the tribological, electrical, thermal, and mechanical properties of metals [25, 26].

Among the various reinforcement element used, zirconia is one of the most effective accessible materials. It has superior wear resistance and the ability to gain good mechanical properties at a high temperature [27]. Zirconia (ZrO_2) has good corrosion and chemical resistance with no absence of brittleness in advanced ceramics. This material's other basic properties include excellent hardness, low wear rate, low friction coefficient, good electrical insulation, and thermal conductivity [28]. Also, zirconia is used in various applications, such as valves, oxygen sensors, pump seals, cutting blades, thread guides, driveshafts, metal forming, and metrology components. For the reasons mentioned above, ZrO_2 nanoparticles are a good candidate for reinforcement elements in AMMCs [29].

Many researchers have investigated the mechanical, tribological properties, and microstructure of Al-graphene [30–39] and Al-ZrO_2 [12, 29, 40–46] nanocomposites. Chen et al. [30] investigated the tensile strength of Al2024-graphene composites with various GNPs amounts (0.5, 0.8, 1, 1.5wt.%) via powder semi-solid processing and friction stir processing. The test results demonstrated that the strength enhanced from 350 MPa (Al2024 alloy) to 524 MPa (Al2024-1wt.%GNPs). Over 1wt.%GNPs contribution ratio, the strength decreased because of the clustered GNPs. AbuShanab et al. [31] researched the Al2024-graphene composites with different graphene amounts (0.25-2wt.%) produced via the mechanical alloying method. The elastic modulus, yield strength, and hardness of Al2024-2%GNPs improved by ~ 155%, ~ 134%, and ~ 97% compared with Al2024 alloy, respectively. A rise in sintering temperature enhanced the mechanical strength and microstructure of the prepared samples. Shin et al. [32] focused on the thermal and mechanical properties of Al2024 alloy, Al2024-5%carbon nanotube, Al-5%graphene composites. The results indicated that the strength of the prepared composites is ~ 2.5 times higher than those of the Al2024 alloy. The thermal expansion coefficient of Al-carbon nanotube and Al-graphene composites is ~ 20% lower than Al2024 alloy. Zheng et al. [33] examined the properties of graphene nanoplatelets reinforced aluminum composites. Test results showed that the yield

strength and ultimate tensile strength of Al-5vol.%GNPs are 62% and 60% higher than those of aluminum. The improved mechanical strength was attributed to the effective load transfer capacity of graphene. Chak and Chattopadhyay [34] researched the tensile strength, hardness, and heat-treatment effect of Al7075-GNPs composites. An increase of 37% in tensile strength and 27% in hardness of Al7075-0.3%GNPs was detected as compared to cast Al7075 alloy. Also, heat treatment causes an improvement of 83% and 34% in hardness and tensile strength compared with the heat-treated Al7075 alloy. Yu et al. [35] focused on the physical properties and mechanical strength of Al-5wt.%GNPs composite and pure Al. The results indicated that the yield strength, hardness, and fracture strain of Al-5wt.%GNPs composite were determined as 248 MPa, 73 HV, and 16%, respectively. Also, the yield strength of the composite was obtained as ~ 65% higher than pure aluminum. Khan et al. [12] investigated the mechanical strength of Al-ZrO_2-SiC composites produced. SiC nanoparticles' content was certain as 5wt.%, while zirconia nanoparticles' contents were varied from 3 to 9wt.% to research the mechanical strength of the fabricated nanocomposites. The best hardness (67 HV), compressive strength (355 MPa), and yield strength (103 MPa) were obtained Al-5%SiC-9%ZrO_2 nanocomposite when compared to pure Al and other fabricated composites. Boppana et al. [29] studied the microstructure and mechanical strength of Al6061 alloy, Al6061-1%ZrO_2-0.5%GNPs, and Al6061-1%ZrO_2-0.75%GNPs nanocomposites. Compared to Al6061 alloy, the yield strength and tensile strength of Al6061-1%ZrO_2-0.75%graphene nanocomposites improved by ~ 42.2% and ~ 38.9%, respectively. Pandiyarajan et al. [40] researched the tribological and mechanical behavior of Al6061-ZrO_2-graphite composites fabricated with 2, 6wt.% ZrO_2 and graphite content by the stir casting method. An increase in ZrO_2 content improved wear resistance, hardness, and tensile strength compared to Al6061 alloy. Also, an increase in graphite content from 2wt.% to 6wt.% decreased the mechanical strength and wear resistance. Kumar et al. [41] focused on the physical, mechanical, and tribological properties of Al6061-ZrO_2 nanocomposites. Four casts of various reinforcement ratios vary between 0wt.% and 6wt.% were produced using the stir casting method. The test results demonstrated that hardness and tensile strength improved by ~ 66% and ~ 90% compared to Al6061 alloy. Volumetric wear decreased from 20 mm^3 (Al6061 alloy) to 4 mm^3 (Al6061-6ZrO_2) for a load of 10 N and a sliding distance of 1.5 km. Wear experiment findings indicate that an increase in nano-ZrO_2 content improved the wear resistance of the fabricated composites.

According to the literature research, although many studies are available related to the mechanical and tribological properties of Al-graphene and Al-ZrO_2 nanocomposites, those properties of Al-ZrO_2-graphene nanocomposites have

not been examined. Since the powder metallurgy route has a remarkable effect on the microstructural, tribological, and mechanical behaviors of Al hybrid nanocomposites, it is thus realistic to investigate the production of graphene and ZrO_2 reinforced Al hybrid nanocomposites through the powder metallurgy method to research these properties. In order to rectify the deficiency of the papers on the influence of the ZrO_2/GNPs content on the tribological and mechanical properties of Al hybrid nanocomposites, a detailed investigation of the effect of the ZrO_2/GNPs contents on the tribological, mechanical properties, and microstructure of Al hybrid composites is also stated in this paper. This study will be the first paper on the fabrication of GNPs-ZrO_2 Al nanocomposites using the powder metallurgy route. The intended properties of binary ZrO_2 and GNPs reinforced Al nanocomposites confirm their development and their potential. Also, prepared Al-ZrO2-GNPs composites may be used in various engineering applications such as driveshafts, valves, pump seals, thread guides, metrology components, gears, and bearings.

2 Experimental

2.1 Matrix and Reinforcing Materials

Pure Al was chosen as the main material for the present examination due to its uses in the aviation and automotive industries. It was strengthened with graphene and ZrO_2. Pure aluminum has a purity of 98%, an average particle size of ~ 10 μm, and a theoretical density of 2.7 g/cm^3. Zirconia (ZrO_2) varied between 1wt.% and 12wt.%, and graphene changed between 0.15wt.% and 0.45wt.% for developing Al-ZrO_2-GNPs hybrid nanocomposites. Pure aluminum, ZrO_2, and graphene powders were supplied by Alfa Aesar, Merck, and Grafen Chemical Industries, respectively.

The reinforcement element for this study was preferred as ZrO_2 due to its excellent properties, such as excellent wear resistance and high hardness. The zirconium's density is 5.67 g/cm^3, and the melting point is more than 2600 °C. In this investigation, zirconium was supplied as a powder with a 70 nm size. Graphene was considered as the other strengthening material because of its lightweight, high Young's modulus, high electron mobility, and high thermal conductivity. In this paper, graphene has a 5–8 nm thickness, a 5–10 μm diameter, and a 2.25 g/cm^3 theoretical density.

2.2 Preparation of the Composites

The powder metallurgy (PM) route was utilized in this work to fabricate Al-ZrO_2, Al-ZrO_2-graphene, and pure aluminum (Fig. 1). Firstly, pure aluminum powders were mixed in ethanol solution for 60 min. At the same time, nanozirconia and nanographene were ultrasonicated in ethanol

solution. Afterward, nano-zirconia–graphene–ethanol solution was added to Al-ethanol solution little by little. The solution was mixed by high-energy ball milling. In this process, the mixture time and mixture speed were determined as 3 h and 250 rpm, respectively. Subsequently, the mixture was dried at 50 °C for 18 h and filtered under a vacuum to remove the ethanol. The mixed powders were pressed in a mold by a single axial press under 700 MPa pressure. After pressing, the green bodies have a $10 \times 10 \times 5$ mm size. These samples were sintered at 630 °C for 3 h under vacuum. The sintered bodies were grinded with the papers (400, 1200, 2500 grit) and then polished with a diamond past of a size of 1 μm to obtain a mirror surface [37–39].

The apparent densities of the developed bodies may be expressed based on Archimedes' principle by the following equation [37].

$$\rho_D = [m_K/(m_D - m_A)] \times \rho_W \tag{1}$$

where ρ_W is defined as the water's density, m_K, m_A, and m_D are the sample's mass, the submerged sample's mass in water, the water-saturated specimen's mass, respectively.

Considering the theoretical density of ZrO_2 ($\rho_{ZrO2} = 5.67$ g/cm^3), graphene ($\rho_{Gr} = 2.25$ g/cm^3), and pure Al ($\rho_{Al} = 2.7$ g/cm^3), the theoretical density (ρ_T) of the developed bodies may be calculated as follows [37].

$$\rho_T = (m_{ZrO2}\% \times \rho_{ZrO2}) + (m_{Gr}\% \times \rho_{Gr}) + (m_{Al2024}\% \times \rho_{Al2024}) \tag{2}$$

where $m_{ZrO2}\%$, $m_{Gr}\%$, and $m_{Al}\%$ are the mass fraction of ZrO_2, graphene, and pure Al.

The fraction of the apparent density to the theoretical density of the specimens was expressed as the relative density of the specimens. By considering the relative–density, the porosity (P%) may be calculated by the following equation [37].

$$P\% = (1 - \rho_D/\rho_T) \times 100 \tag{3}$$

Micro-Vickers hardness values were detected by the Vickers hardness test device (HV-1000B) with load applied 200 g for 15 s. The presented values are a mean of eight measurements for each specimen. The compressive strength of Al-ZrO_2, pure Al, and Al-ZrO_2-GNPs composites was determined via the Mares tst-10t compressive testing machine with a 5 mm/min speed.

Tribological properties of the developed materials such as wear loss, mass loss, sliding distance, and the friction coefficient among particles may be explained by a pin-on-disk wear test device. One of those parameters is the sliding distance (L) which varies with the abrasive disk's (440C stainless steel disk) radius (R = 20 mm), number of revolutions (n
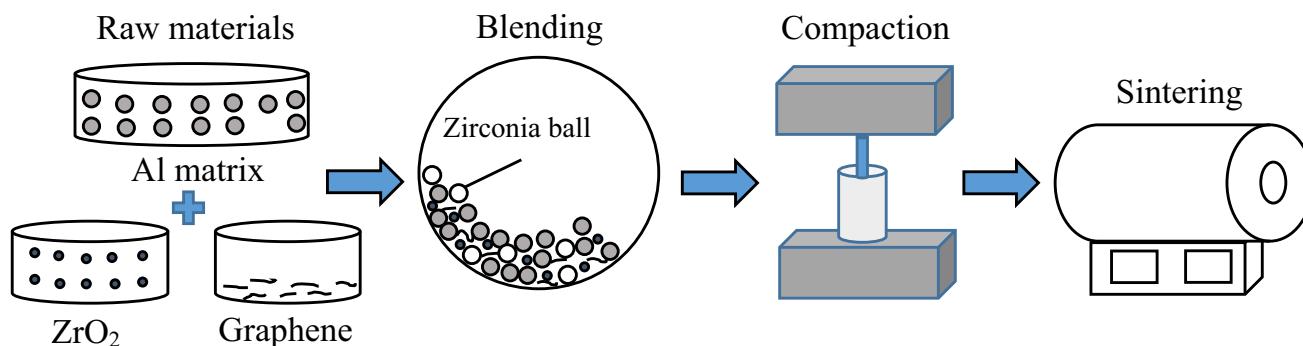
Fig. 1 Schematic representation of the fabrication of Al-ZrO2-graphene nanocomposites

= 200 rpm), and testing time (t = 20 min) as given in the following equation:

$$L = 2 \times \pi \times R \times n \times t \tag{4}$$

As a result of considering the test parameters, L may be calculated as.0.5 km. The worn surface's volume (ΔV) may be expressed by the ratio of mass loss (Δm) to the apparent density (ρ) of the specimen as given below:

$$\Delta V = \Delta m / \rho_D \tag{5}$$

The wear rate (W, mm^3/(Nm)) of specimens may be defined by considering the applied load (P, N) and sliding distance (L, m) as follows [47]:

$$W = \Delta V / (L \times P) \tag{6}$$

According to Archard's equation, the volume of the worn surface (ΔV) has a relation with the hardness, which may be described as follows [47, 48]:

$$\Delta V = P \times \mu \times L / H \tag{7}$$

where μ is the coefficient of friction and H is the hardness. Regarding the wear rate variation with an applied load in the literature, Archard's equation shows the wear rate is proportional to the applied load [47, 48].

The particle size distribution of ZrO_2 and pure Al were detected by the particle size measurement device (Malvern Mastersizer 3000). The XRD investigations were performed on the powders and sintered samples (Rigaku Smartlab model) with a 0.02° scanning rate recorded in a range of $2\theta = 20$–$80°$. The XRD device had a 0.154 nm wavelength, 40 kV, and 150 mA operation conditions. SEM device (Jeol JSM 7001F) was utilized to investigate the microstructure of powders and composites. Besides, SEM–energy-dispersive X-ray (EDX) spectroscopy investigations were employed to examine the ZrO_2 and graphene nanoparticles' distribution in the microstructure.

3 Results and Discussion

3.1 Powder Characterization

XRD patterns of graphene, ZrO_2, and pure aluminum powders are demonstrated in Fig. 2. As given in the figures, graphene (01-0646 of JCPDS card no), ZrO_2 (37–1484 of JCPDS card no), and pure Al (01-1180 of JCPDS card no) are expected at $2\theta = \sim 26.8°$; $2\theta = \sim 28.2°$, 31.5°, 33.8°, 38.5°, 41.2°, 45.4°, 50.1°, 56.3°, 59.8°, 62.7°, 65.4°, 71.2°, 74.8°, 78.3°; and $2\theta = \sim 38.8°$, 45.2°, 65.3°, 77.8°, respectively. These X-ray diffraction analyses are an excellent technique to describe the XRD patterns of the developed samples.

Figure 3a–c demonstrates the SEM images of nanographene, nano-ZrO_2, and pure Al powders. As given in Fig. 3a, nanographene had a two-dimensional structure, irregularly shaped flakes, and a stack-like morphology. Additionally, the thickness of graphene nanolayers was detected as less than 100 nm. ZrO_2 nanoparticles had a spherical morphology with less than the size of 100 nm (Fig. 3b). On the other hand, pure Al powders had an irregular shape with less than the size of 20 μm (Fig. 3c). In order to determine the mean particle size of pure Al and ZrO_2, particle size distribution was performed by Malvern Mastersizer 3000 laser particle size analyzer. As illustrated in Fig. 3d and e, the mean particle sizes of pure Al and ZrO_2 were measured as ~ 10 μm and ~ 70 nm, respectively. The results of these analyses were verified with the SEM images of powders.

3.2 Physical Properties of the Prepared Specimens

The porosity and apparent density variations of Al-ZrO_2-graphene and Al-ZrO_2 composites were exhibited in Fig. 4. The specimens' densities were determined by Archimedes' method. It depends on many parameters like particle shape, particle size distribution, agglomeration tendency of particles, friction between particles, sintering temperature and time, reinforced powder amount. As illustrated in Fig. 4a, an
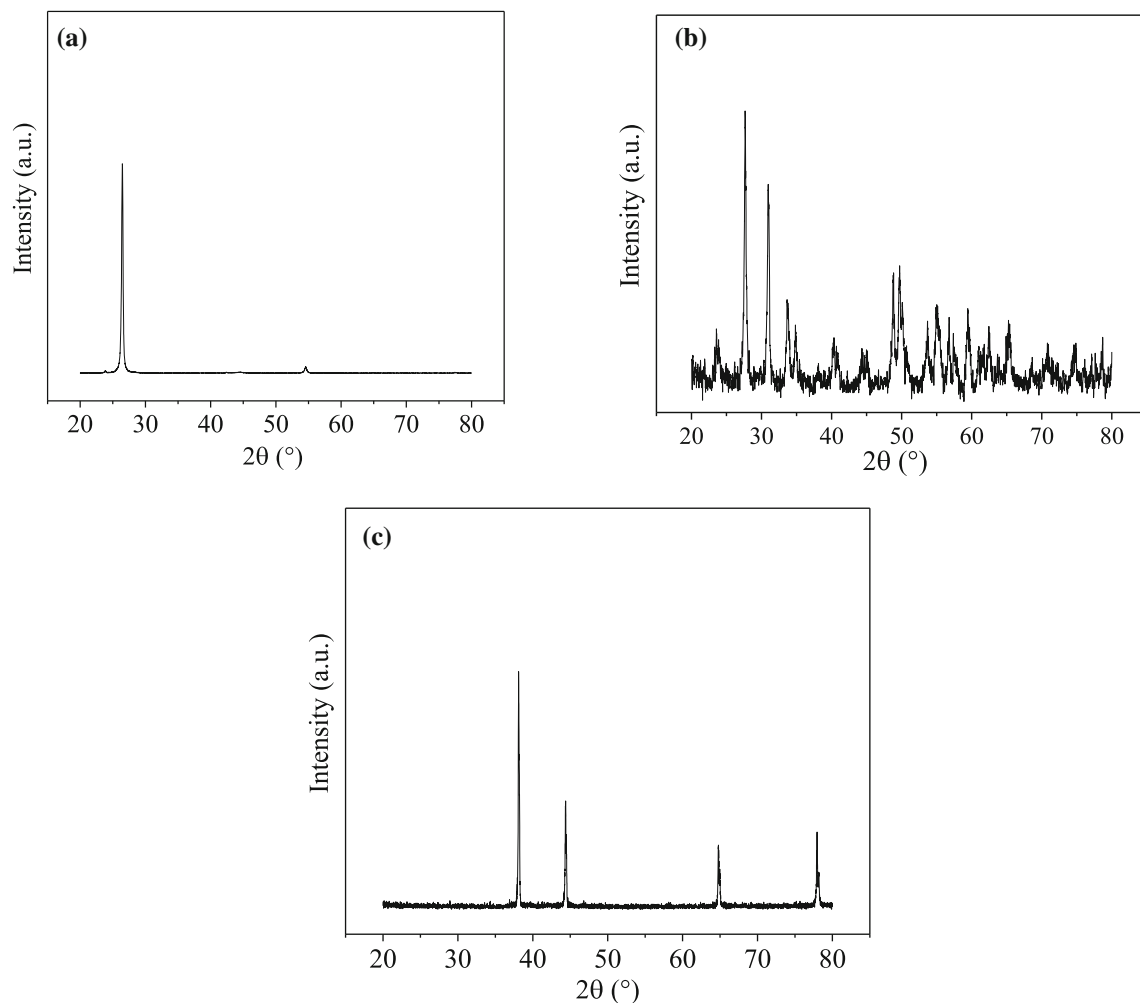
Fig. 2 XRD plots of the powders: **a** graphene, **b** ZrO_2, and (**c**) pure Al

increase in nano-ZrO_2 amount enhanced the apparent density up to 9wt.%ZrO_2 content. Surprisingly, the apparent density decreased due to clustered ZrO_2 nanoparticles in the case of over 9wt.%ZrO_2 content. The highest density was measured as 2.84 g/cm^3 among fabricated Al-ZrO_2 composites. By considering 9wt.%ZrO_2 content, Al-9ZrO_2-xGraphene composites (x = 0.15, 0.30, 0.45wt.%) were produced by the PM method. As given in Fig. 4b, maximum density (2.86 g/cm^3) was obtained at the Al-9ZrO_2-0.15GNPs. Over 0.15%GNPs amount, the clustered GNPs caused a decline in the density of the Al hybrid composites. Figure 4c and d shows the porosity variation of Al-ZrO_2 and Al-ZrO_2-graphene composites. As indicated in the figures, the homogeneous distributions of nano-ZrO_2 and nanographene particles positively affected to decrease in the porosity of Al-ZrO_2 and Al-ZrO_2-graphene composites. Similarly, minimum porosity was reached Al-9ZrO_2 (4.3%) and Al-9ZrO_2-0.15GNPs (3.7%) composite. As illustrated in these figures, GNPs and ZrO_2 amounts have

a significant role in the density and porosity of the prepared composites. The uniform distribution of nano-ZrO_2 and nanographene particles is limited to over 0.15%GNPs and 9%ZrO_2 amounts due to the clustered nanoparticles. As a result, the rearrangements of the particles are denied, and GNPs and ZrO_2 nanoparticles are not embedded in Al powders. Moreover, these clustered nanoparticles decrease the contact area among Al particles. This situation leads to higher porosity and lower density [49]. There are some valuable studies in which the effect of agglomerated graphene is noted. Li et al. [50] and our previous paper [39] indicated the higher mechanical properties and higher density for low graphene/ceramic content, whereas the mechanical strength of graphene reinforced aluminum composites deteriorated in the case of over 0.2wt.%graphene and 9wt.%Si_3N_4 contents because of the agglomerated nanoparticles.
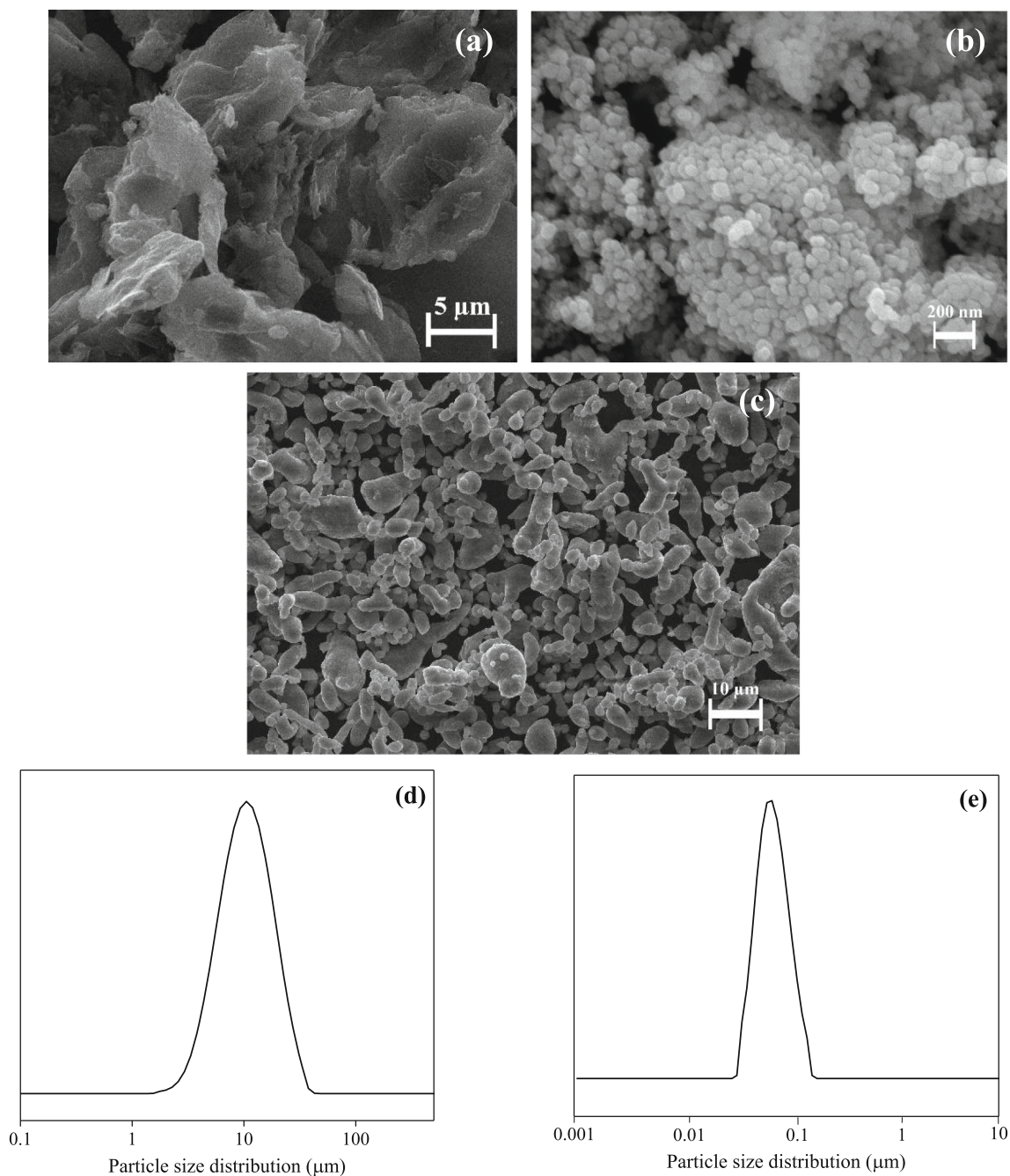
Fig. 3 SEM images of the powders: **a** graphene, **b** ZrO_2, **c** pure Al and particle size distribution of the powders: **d** pure Al, **e** ZrO_2

3.3 Mechanical Properties of the Prepared Specimens

Figure 5 gives the micro-Vickers hardness values of Al-ZrO_2-GNPs and Al-ZrO_2 composites. It was found to enhance from 30 ± 1.2 to 69 ± 1.2 HV with rising ZrO_2 amount from 0 to 9wt.% (Fig. 5a). As already known that zirconia is an extremely hard material among other ceramics. There is a big hardness difference between Al and zirconia. Hence,

an incredible enhancement of composite's hardness by the addition of zirconia is observed. The better hardness values are proof by a homogeneity distribution of ZrO_2 nanoparticles up to 9wt.%ZrO_2. Thus, the ZrO_2 addition to the matrix has a considerable effect on the specimen's hardness. The effect of GNPs amount on the hardness of the ZrO_2-GNPs reinforced Al matrix composites is presented in Fig. 5b. The hardness enhanced from 69 ± 1.2 HV (Al-9ZrO_2) to 75 ± 2 HV (Al-9ZrO_2-0.15GNPs). A significant
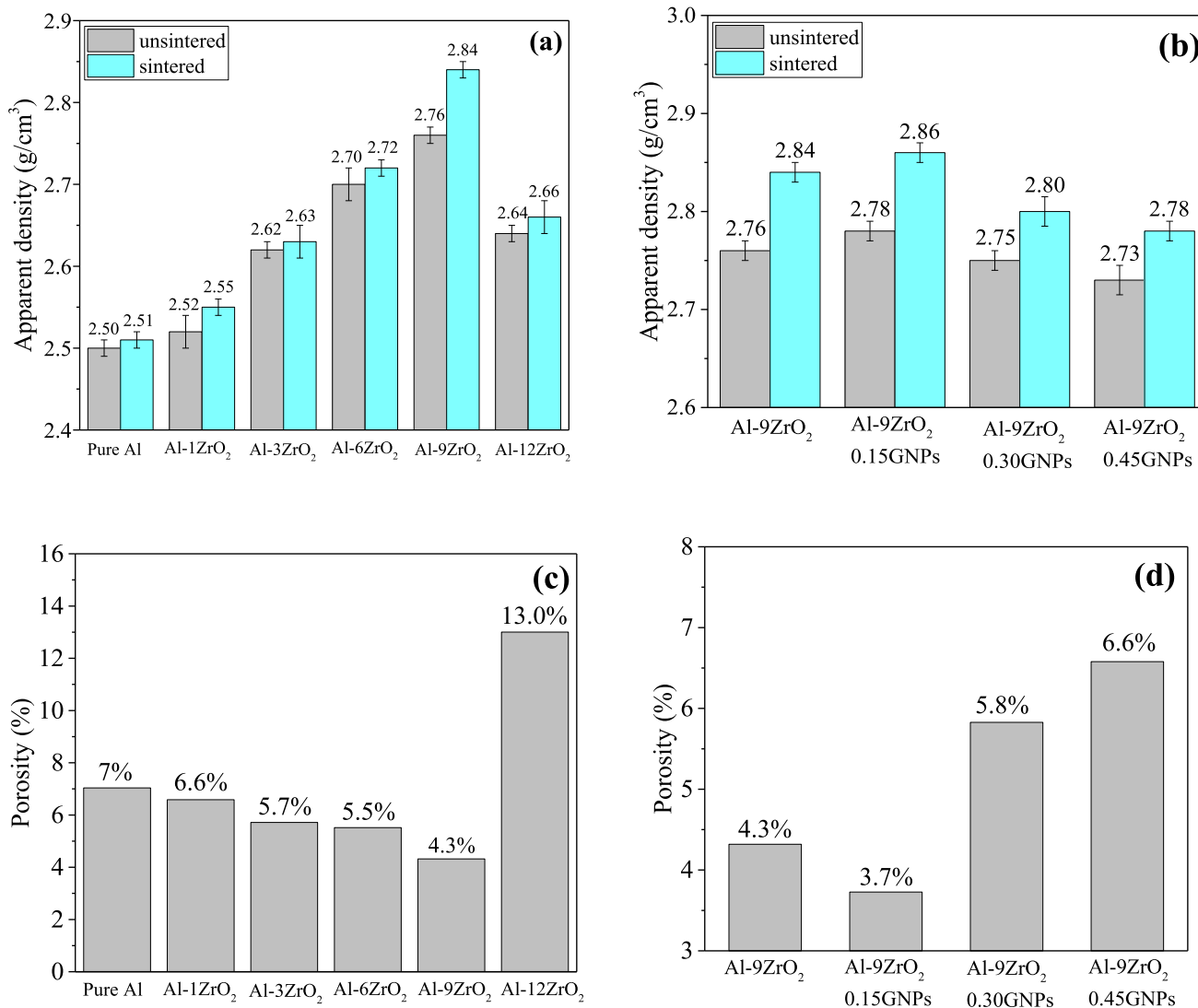
Fig. 4 The apparent density variation of the composites: **a** Al-ZrO₂, **b** Al-ZrO₂-graphene; porosity variation for sintered composites: **c** Al-ZrO₂, **d** Al-ZrO₂-graphene

increment (150%) for 0.15%GNPs-9%ZrO₂ reinforced Al matrix was detected compared with the hardness of pure Al. The Vickers hardness of Al hybrid composites enhanced up to 0.15wt%GNPs amount because of high surface area and homogeneous distribution of graphene. In the case of over 0.15wt.% graphene amount, graphene nanoparticles were clustered due to their electrostatic forces and nanostructure among the particles. It caused easy sliding between graphene nanoparticles over 0.15wt.% during plastic deformation. In other words, graphene lost the enhancement effect and acted as a solid lubricant during deformation. This deterioration in the hardness due to the agglomeration of graphene was observed in many relevant studies [6, 9]. Similarly, ZrO₂ nanoparticles acted as graphene nanoparticles over 9wt.%ZrO₂ content. These excessive contribution rates of ZrO₂ and graphene led to a decrease in the hardness of

Al matrix composites due to their difficult dispersion in the microstructure. To expose the clustered ZrO₂ and graphene nanoparticles, SEM–EDX and SEM analyses of aluminum hybrid composites were performed by the SEM device.

Al matrix composites' hardness may be improved by the contribution of ZrO₂ and graphene nanoparticles. Equation (8) implied the enhancement in the hardness based on the rule of the mixtures [1, 51].

$$H_c = H_m f_m + H_r f_r \tag{8}$$

where f_r and f_m are the reinforcement and matrix elements' volumetric rates, H_r and H_m are the reinforcement and matrix elements' hardness.

The strength of the dislocation can be explained by the density mechanism of the dislocation. It controls the
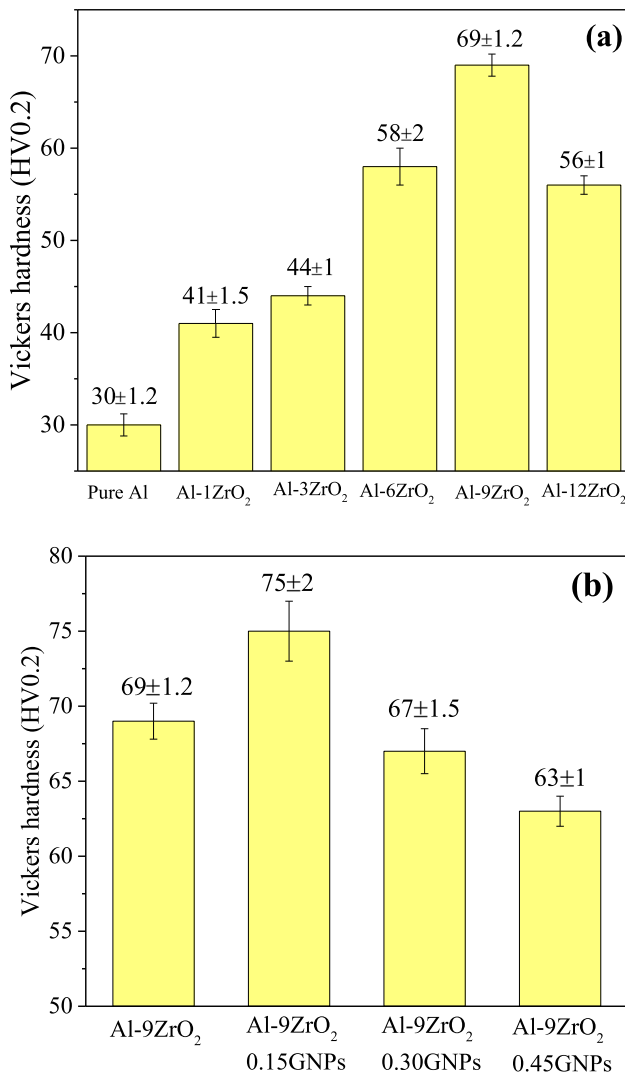
Fig. 6 The compressive strength variation of pure Al, Al-ZrO$_2$, and Al-ZrO$_2$-graphene composites

Fig. 5 The Vickers hardness variation of sintered composites: **a** Al-ZrO$_2$, **b** Al-ZrO$_2$-graphene

nanoparticles. In the case of over 9wt.%ZrO$_2$, the compressive strength sharply decreased to 250 ± 5 MPa (Al-12ZrO$_2$) due to the agglomerated ZrO$_2$ nanoparticles. By selecting 9wt.%ZrO$_2$, the compressive strength of the Al-9ZrO$_2$-x%graphene (x = 0.15, 0.30, 0.45wt.%) composites was examined. Among aluminum-based composites, the highest compressive strength was detected Al-9ZrO$_2$-0.15GNPs composite (490 ± 4 MPa). A significant enhancement (~ 163%) in the strength of the Al-9ZrO$_2$-0.15graphene composite was determined compared with pure aluminum. In the case of over 0.15wt.%graphene content, the compressive strength declined because of easy sliding during deformation and agglomerated nanographene. The weak interfaces between graphene and Al formed due to the agglomerated nanographene. They led to too low strength and too high porosity [38, 49, 50].

An increase in graphene and ZrO$_2$ nanoparticles contents in the Al matrix causes the decline in the distance among the particles (λ) as shown in the following equations [1, 51]:

$$\lambda = [4r(1 - f)]/(3f) \tag{10}$$

where r is the nanoparticles' radius, λ is the distance among the reinforcing nanoparticles, and f is the nanoparticles' volume fraction. The shear stress (τ_0) may be expressed as follows [1, 51]:

$$\tau_0 = bG/\lambda \tag{11}$$

where G is the shear module. The decrease in the distance between graphene and ZrO$_2$ nanoparticles will increase the tension during the dislocation motion among these nanoparticles, which causes an improvement in the shear strength. Hence, the composite's strength enhances [52–54].

composites' hardness. The addition of graphene and ZrO$_2$ nanoparticles to the matrix improved the dislocation density because of the nanosized ZrO$_2$ and graphene particles. A rise in the density of the dislocation causes the improvement of Al hybrid composites. Equation (9) expressed the improvement in hardness for ZrO$_2$ and graphene reinforced Al matrix composites with the contribution of ZrO$_2$ and GNPs nanoparticles. [1, 51].

$$H = Gb\alpha\sqrt{\rho} + h\sqrt{tD} \tag{9}$$

where α, G, h are the constant and b is Burger's vector.

Figure 6 gives the compressive strength variation of Al-ZrO$_2$-graphene and Al-ZrO$_2$. As shown in the figure, the compressive strength improved from 186 MPa (pure Al) to 287 MPa (Al-9ZrO$_2$) with the reinforcement of ZrO$_2$
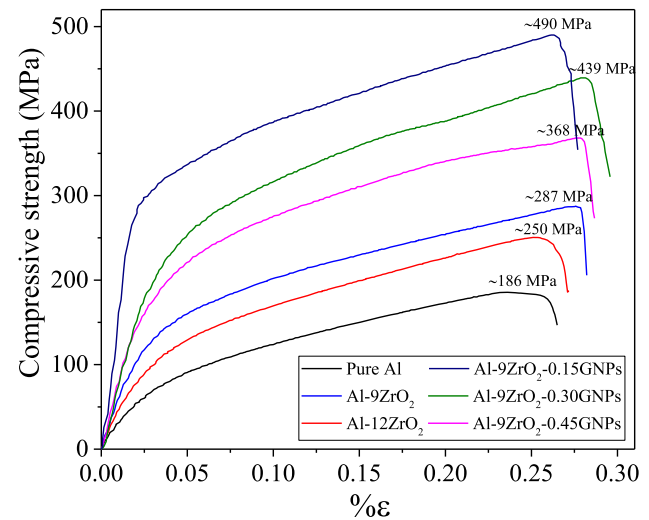
The movement of the dislocations is a significant state in terms of reinforcement of the particles. Graphene and ZrO_2 nanoparticles act as a barrier in the Al matrix. Besides, these nanoparticles cause dislocations' bending while limiting the movement of the dislocation during plastic deformation. When the reinforcing nanoparticles are inserted into the matrix, the distance among particles decreases, and then the dislocations' movement gets hard because they encounter more barriers, and the pile-up of the dislocations occurs. This enhancement effect is confirmed by some valuable studies [55, 56]. The enhancement in the composite's strength may be described as given below [53–56].

$$\sigma_c = f_r \sigma_r + f_m \sigma_m \tag{12}$$

where f_m is the matrix element's volume fraction, and f_r is the reinforcing element's volume fraction. σ_m is the matrix element's strength, σ_r is the reinforcing element's strength, and σ_c is the composite's strength.

XRD plots of Al-9ZrO$_2$ and Al-9ZrO$_2$-0.45GNPs composites are given in Fig. 7a. From these plots, it may be seen that Al-9ZrO$_2$-0.45GNPs composites have aluminum ($2\theta = \sim 38.8°$, $45.2°$, $65.3°$, $77.8°$) and ZrO$_2$ ($2\theta = \sim 28.2°$, $31.5°$, $33.8°$, $38.5°$, $41.2°$, $45.4°$, $50.1°$, $56.3°$, $59.8°$, $62.7°$, $65.4°$, $71.2°$, $74.8°$, $78.3°$) peaks. Also, ZrO$_2$ peaks can be observed an enlarged pattern of Al-9ZrO$_2$-0.45GNPs composite (Fig. 7b). The peak of graphene ($26.8°$) was not occurred in an XRD plot of Al-9ZrO$_2$-0.45GNPs composite because of its minimal presence in the microstructure. In order to determine graphene's existence in Al hybrid composite, SEM and SEM–EDX analyses were carried out. Moreover, undesired secondary phases (Al$_4$C$_3$, etc.) were not determined in any ZrO$_2$ and GNPs reinforced aluminum-based composites, because this undesired phase structure might reduce the improvement effect of graphene nanoparticles on the mechanical properties of the Al matrix composite.

Figure 8 illustrates the high magnification SEM images of Al-ZrO$_2$, Al-ZrO$_2$-graphene composites, and pure aluminum. As shown in Fig. 8a–g, aluminum particles were sintered by well-bonding and the formation of a strong neck. The fracture surface analyses of Al-9ZrO$_2$ (Fig. 8b) and Al-9ZrO$_2$-0.15grapene (Fig. 8d) showed that ZrO$_2$ and graphene nanoparticles were distributed homogeneously. Also, good bonding and strong interface between particles were detected by high magnification ($\times$ 40,000) SEM image of Al-9ZrO$_2$-0.15GNPs composite (Fig. 8g). From the SEM images of Al-12ZrO$_2$ (Fig. 8c), Al-9ZrO$_2$-0.30graphene (Fig. 8e), Al-9ZrO$_2$-0.45graphene (Fig. 8f), clustered graphene and ZrO$_2$ nanoparticles were observed in the case of over 9wt.%ZrO$_2$ and 0.15wt.%graphene amount. These clustered nanoparticles deteriorated the mechanical strength of the prepared Al-ZrO$_2$ and Al-ZrO$_2$-graphene composites. As a result of all SEM investigations, the microstructures of Al-ZO$_2$ and
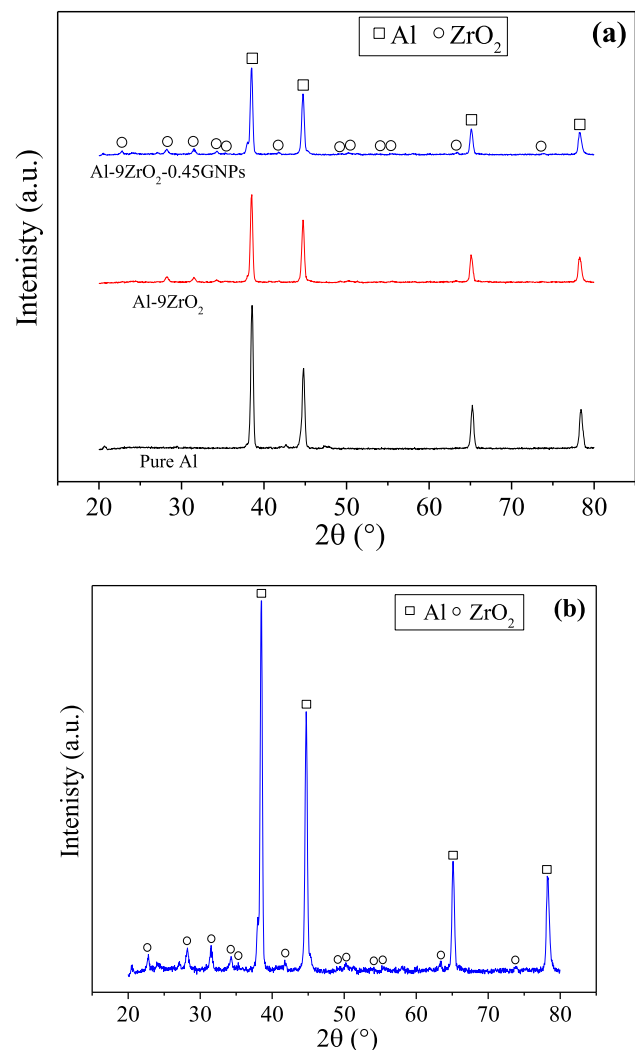

Fig. 7 X-ray diffraction plots of sintered samples: **a** pure Al, Al-ZrO$_2$ and Al-9ZrO$_2$-0.45GNPs composites and **b** an enlarged pattern of Al-9ZrO$_2$-0.45GNPs composites

Al-ZrO$_2$-graphene composites were verified by the compressive test results.

To show the distribution of ZrO$_2$ and graphene nanoparticles, SEM–EDX mapping analyses of Al-9ZrO$_2$-xGraphene composites (x = 0.15, 0.30, 0.45wt.%) were performed. As seen from Fig. 9a–f, carbon and zirconia signals came from the existence of graphene and ZrO$_2$ nanoparticles, respectively. Also, ZrO$_2$ nanoparticles had a uniform distribution in the Al hybrid composites' microstructure. As illustrated in the SEM–EDX images of the Al-9ZrO$_2$-0.15GNPs composite, graphene nanoplatelets were positioned at the grain boundaries of aluminum without any clustering (Fig. 9a and b). Graphene nanoparticles near the aluminum particles blocked the grain growth during the heat treatment. Moreover, the particles in the Al matrix were refined in small grain sizes without coarsening for the Al particles. It caused an
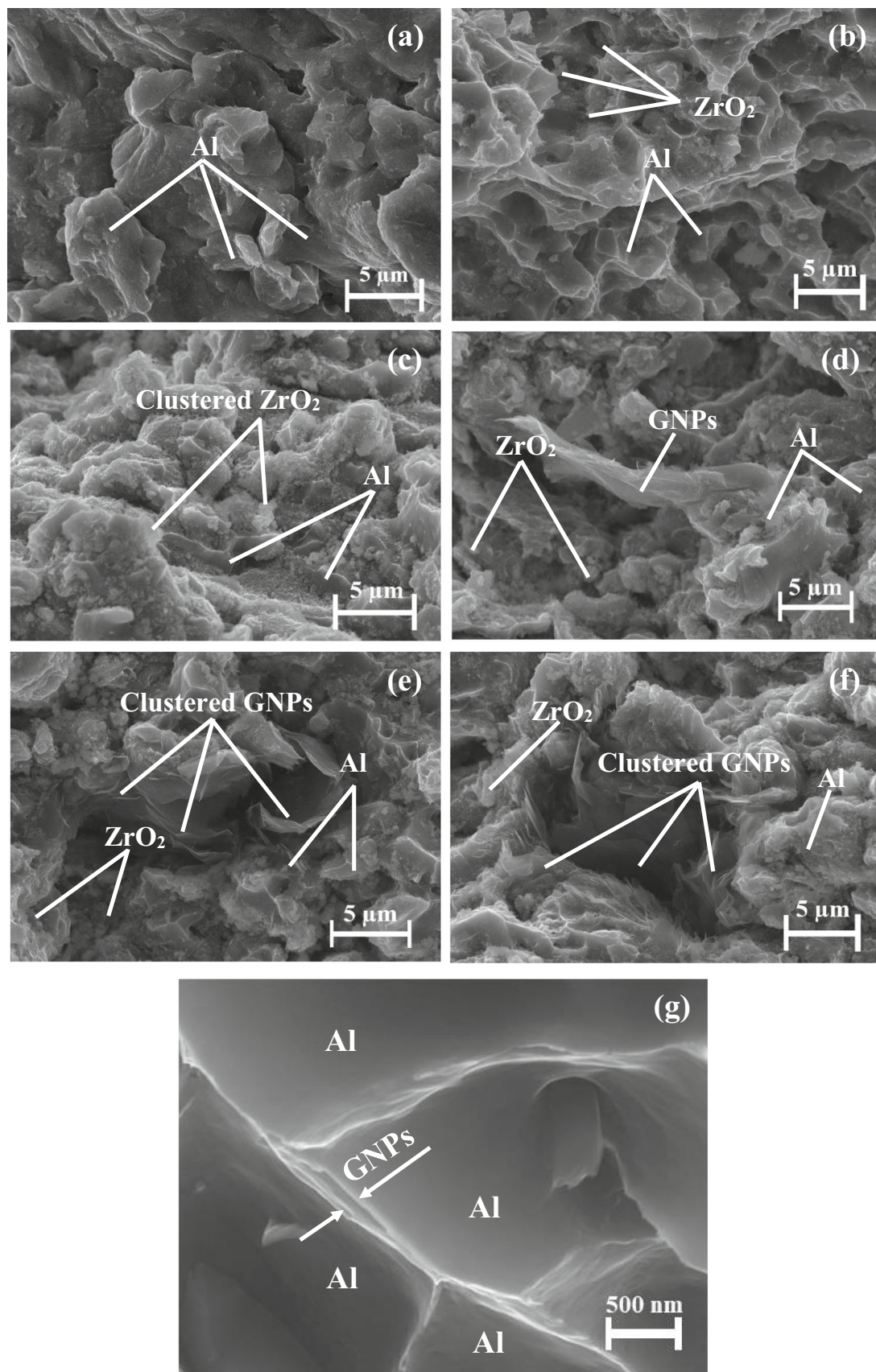
Fig. 8 SEM images of the prepared specimens: **a** pure Al, **b** Al-9ZrO$_2$, **c** Al-12ZrO$_2$, **d** Al-9ZrO$_2$-0.15GNPs, **e** Al-9ZrO$_2$-0.30GNPs, **f** Al-9ZrO$_2$-0.45GNPs, **g** Al-9ZrO$_2$-0.15GNPs (high magnification, × 40,000)
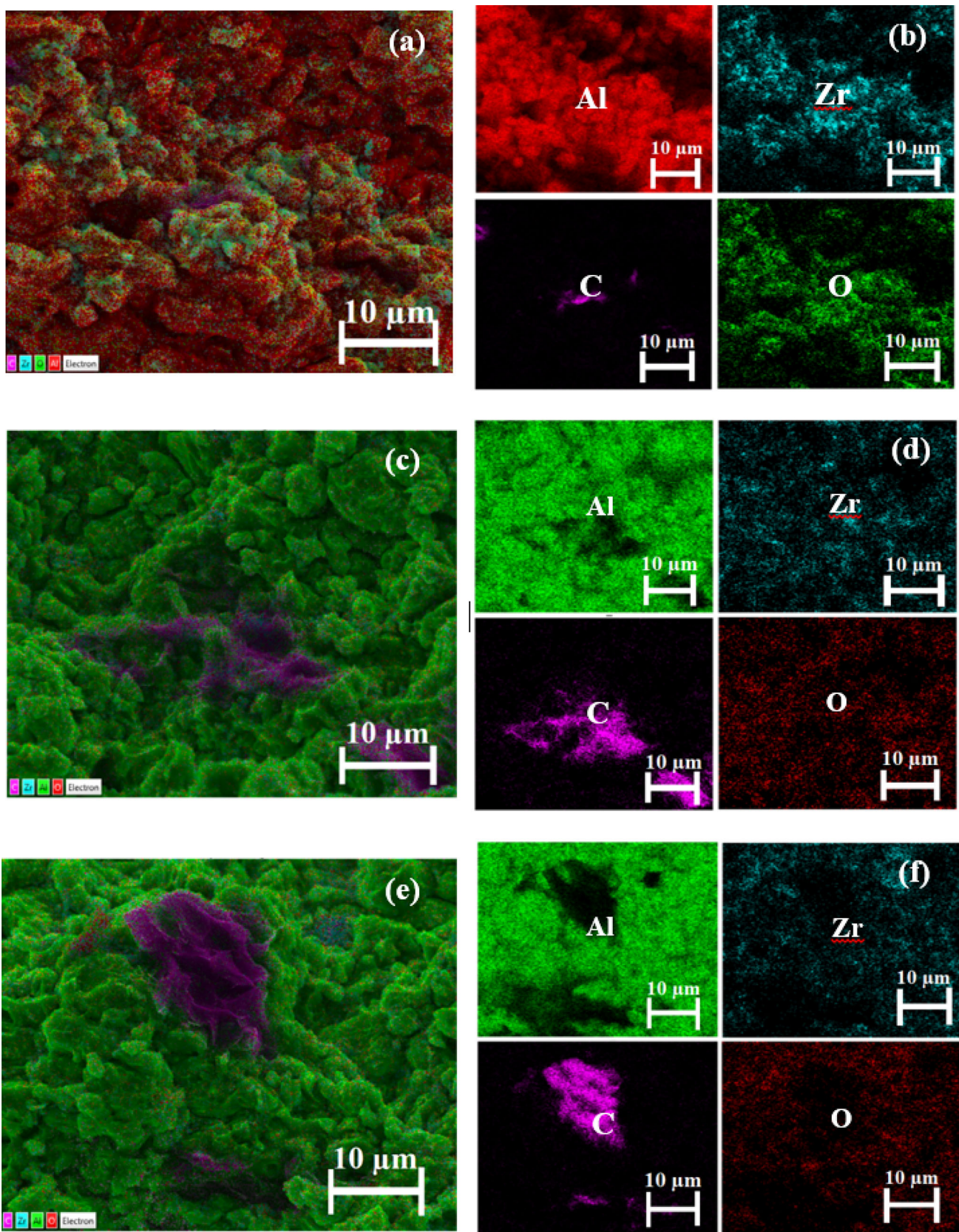
Fig. 9 SEM–EDX images and element distribution of Al hybrid composites: **a**, **b** Al-9ZrO$_2$-0.15GNPs, **c**, **d** Al-9ZrO$_2$-0.3GNPs, **e**,**f** Al-9ZrO$_2$-0.45GNPs
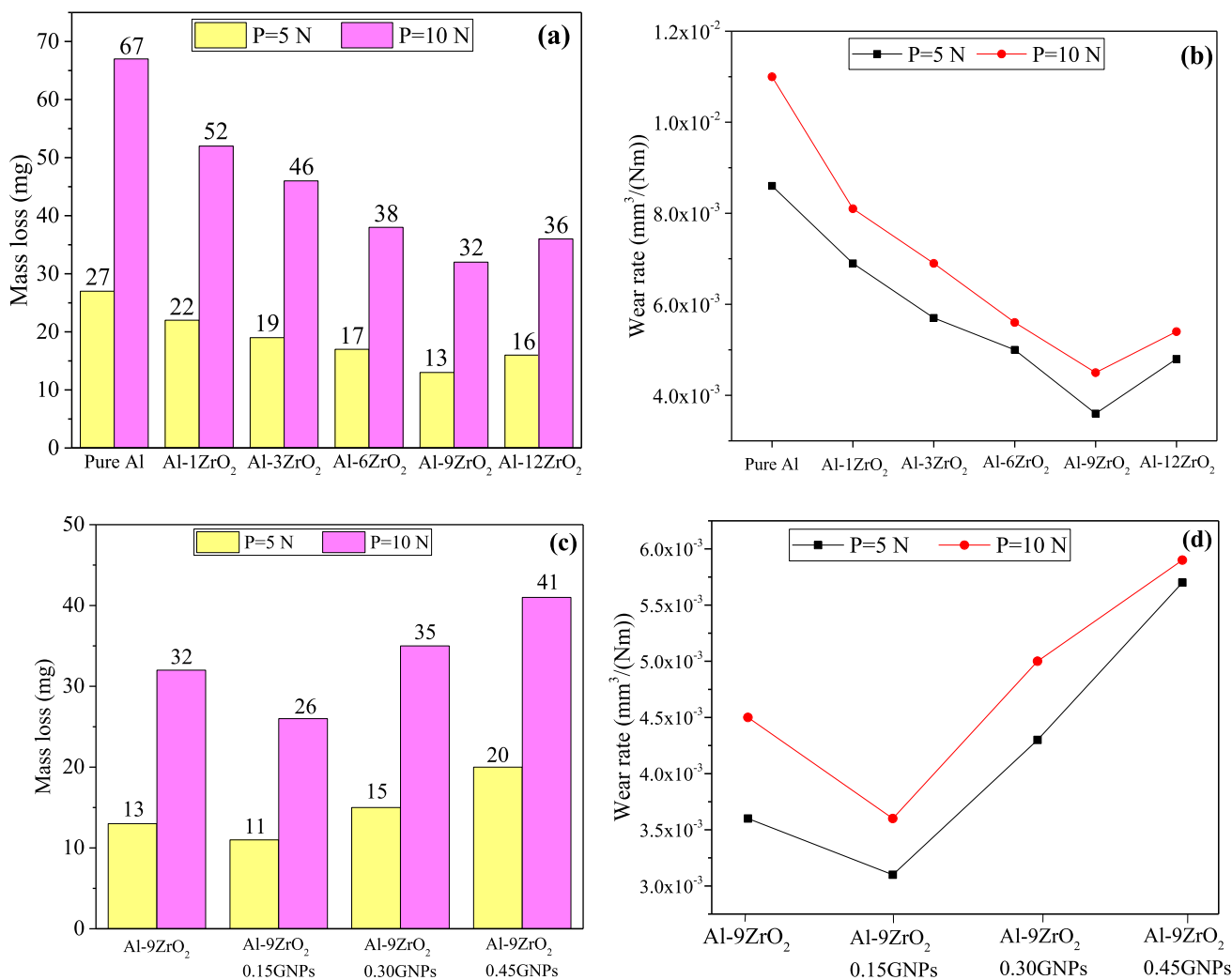
Fig. 10 Mass loss and wear rate variation of the prepared specimens: **a**, **b** Al-ZrO$_2$ and **c**, **d** Al-ZrO$_2$-GNPs composites

enhancement in the physical properties and mechanical properties of the Al-based composites. This phenomenon might be explained by the strengthening of grain refinement. On the other hand, clustered and stacked graphene nanolayers in the SEM–EDX microstructure of Al-9ZrO$_2$-0.30graphene and Al-9ZrO$_2$-0.45graphene composites (Fig. 9c–f) were detected around the Al grains because of the nanosize of graphene. These clustered graphene nanoplatelets caused lower interphase bonding among grains. Hence, too low mechanical strength occurred in Al-9ZrO$_2$-xGraphene composites (x = 0.30, 0.45wt.%).

3.4 Tribological Properties of the Prepared Specimens

Wear rate (W) and mass loss (Δm) variations at a 200 rev/min speed with various loads (P = 5 N and 10 N) during the pin-on-disk wear test for Al-ZrO$_2$-Graphene and Al-ZrO$_2$

composites are shown in Fig. 10. Among Al-ZrO$_2$ composites, minimum wear rate (0.0036 mm^3/Nm) and mass loss (13 mg) were detected Al-9ZrO$_2$ composite for an applied load of 5 N (Fig. 10a and b). It was noticed that the mass loss and wear rate increased with rising the applied load. Also, the rise in ZrO$_2$ amount decreased the mass loss and wear rate up to 9wt.%ZrO$_2$ content due to the hard ceramic structure of ZrO$_2$ nanoparticles. Over 9wt.%ZrO$_2$ amount, the mass loss (Δm) and wear loss (W) increased because of the clustered ZrO$_2$ nanoparticles. In the same way, the lowest mass loss (11 mg) and wear rate (0.0031 mm^3/(Nm)) were obtained with an applied load of 5 N Al-9ZrO$_2$-0.15GNPs composite (Fig. 10c and d). In the case of over 0.15wt.%GNPs amount, the wear rate and mass loss deteriorated due to the clustering tendency of graphene nanoparticles. According to the hardness and wear test results, higher hardness induced enhancement of wear resistance of Al-ZrO$_2$-Graphene composite. The maximum
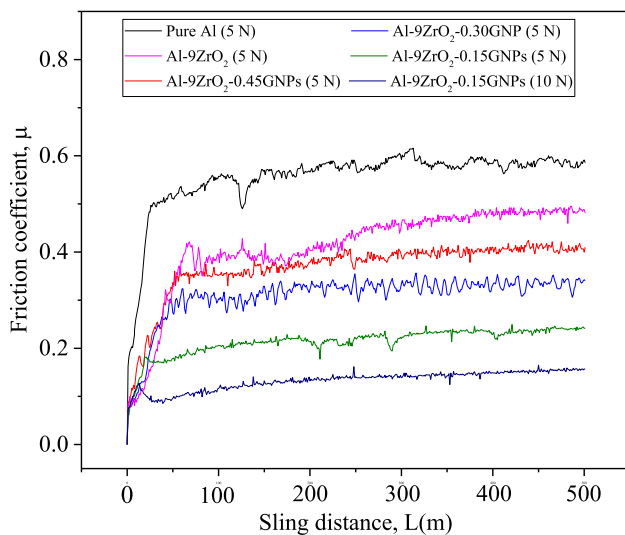
Fig. 11 The coefficient of friction variation between prepared specimens and 440C stainless steel disk

hardness and the minimum wear rate were detected at the Al-9ZrO$_2$-0.15wt.%Graphene composite. In this way, this experiment was confirmed by Archard's equation. The wear test results indicated that graphene nanoparticles were a good solid lubricator due to the graphene's lubricating property [47, 48].

The coefficient of friction variation between prepared specimens and 440C stainless steel disk during the pin-on-disk wear test is illustrated in Fig. 11. At the beginning stage of the wear test, the friction coefficient began to rise for all measurements, which could be caused by the breakdown of surface oxide laminates [57]. All specimens reached the highest value between the distances of 10 m and 30 m during the test. From the wear test, it was seen that the coefficient of friction dropped slightly and then stabilized. Afterward, the rise of the friction coefficient was followed by an abrupt decline after a sliding distance of 30–60 m for the prepared specimens. This situation could be attributed to a sharp drop in the sliding contact area as the articulating surface roughness after obtaining large friction coefficients and, thus, excessive material removal. It was seen that the friction coefficients were fixed over ~ 60 m. The figure showed that the mean friction coefficient decreased from 0.58 ± 0.01 (pure Al) to 0.18 ± 0.01 (Al-9ZrO$_2$-0.15GNPs) with a rise in zirconium and graphene nanoparticles' content. The best coefficient of friction was measured as 0.18 ± 0.01 under an applied load of 10 N Al-9ZrO$_2$-0.15GNPs composite. On the other hand, it was seen that the friction coefficient raised from 0.22 ± 0.01 (Al-9ZrO$_2$-0.15GNPs) to 0.38 ± 0.01 (Al-9ZrO$_2$-0.45GNPs) due to the clustered graphene for an applied load of 5 N. Based on Al-9ZrO$_2$-0.15GNPs composite, the friction coefficient between Al-9ZrO$_2$-GNPs and 440C stainless steel ball decreased from 0.22 ± 0.01 (P = 5 N) to $0.18 \pm$

0.01 (P = 10 N) with increase in the applied load. Otherwise, the rise in the load caused a decrease in the friction coefficient and an increase in the wear rate. The friction coefficient decreased with increase in contact load. Also, the steady-state friction coefficient declined with a rise in applied load, which could be achieved by that the transfer film is destroyed at the increase of loads though more stable at lower loads [58]. Also, the fluctuation of the friction coefficient curves became smaller at relatively higher loads, as reported by other researchers [59]. This situation was caused by the contact area over the asperities tips that are huge [60, 61].

The worn surfaces of Al-ZrO$_2$, Al-ZrO$_2$-GNPs composites, and pure Al after the pin-on-disk wear test were examined under an applied load of 5 N and 10 N by the SEM device. As observed from the worn surface morphologies, the abrasive wear mechanism may be described as the main wear mechanism. Besides, the parallel grooves were detected on the worn surfaces of all specimens. As given in Fig. 12a–g, maximum damage and deepest grooves were determined on the worn surface of the Al specimen (Fig. 12a). It was clearly seen from Fig. 12b and c, the increase in ZrO$_2$ nanoparticles content up to 9wt.% resulted in the decrease in the wear rate due to the hard ceramic structure and uniform distribution of ZrO$_2$ nanoparticles. It was seen that the damage on the surface and shallow grooves increased with increase in the applied load from 5 to 10 N (Fig. 12g). On the other hand, minimum surface damage, minimum wear rate, and minimum friction coefficient were observed at the Al-9ZrO$_2$-0.15GNPs composite under a 5 N load when the worn surface morphologies and wear test results were evaluated together (Fig. 12d). This situation is due to the graphene and zirconium nanoparticles' uniform distribution in the matrix. However, the agglomerations in the case of over 9wt.%ZrO$_2$ and 0.15wt.%graphene nanoparticles deteriorated the wear behavior of Al-12ZrO$_2$ and Al-9ZrO$_2$-0.30GNPs, and Al-9ZrO$_2$-0.45GNPs composites (Fig. 12 c, e, f). Graphene in the Al-based composites acted as a solid lubricator at the interface and enhanced the lubrication effect. Hence, the minimum wear rate (0.0031 mm^3/(Nm)), mass loss (11 mg), and friction coefficient (0.18 ± 0.01) were recorded at the Al-9ZrO$_2$-0.15GNPs composite. In conclusion, it may be indicated that GNPs are a very influential lubricator for ZrO$_2$-GNPs reinforced Al composites.

4 Conclusions

In this work, binary ZrO$_2$ and graphene reinforced Al composites and only ZrO$_2$ reinforced Al composites with various nano-zirconium dioxide (1, 3, 6, 9, 12wt.%) and nanographene (0.15, 0.30, 0.45wt.%) contents were produced via the PM route. The effects of ZrO$_2$ and graphene
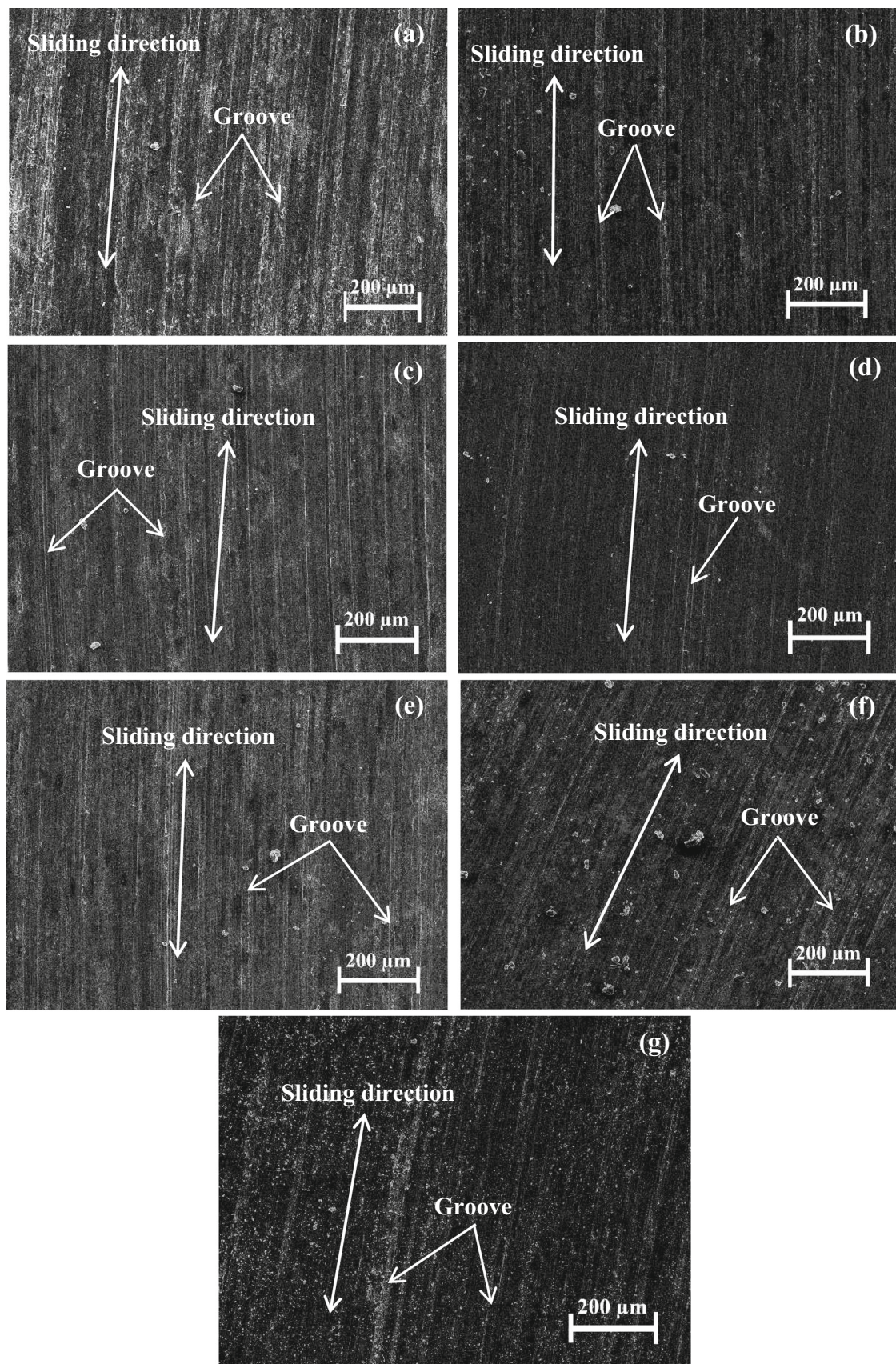
Fig. 12 Worn surfaces of samples: **a** pure Al, **b** Al-9ZrO$_2$, **c** Al-12ZrO$_2$, **d** Al-9ZrO$_2$-0.15GNPs, **e** Al-9ZrO$_2$-0.30GNPs, **f** Al-9ZrO$_2$-0.45GNPs for 5 N load, and **g** Al-9ZrO$_2$-0.15GNPs for a 10 N load

nanoparticles amounts on the porosity, density, compressive strength, mass loss, hardness, wear rate, friction coefficient, and microstructure were investigated. The obtained results were summarized as given below:

(1) From the mechanical and physical test results, the maximum density (2.84 g/cm^3), hardness (75 HV), compressive strength (490 MPa), and minimum porosity (3.7%) were measured at 9wt.%ZrO$_2$-0.15wt.%graphene reinforced Al-based composite. Over 9wt.%ZrO$_2$ and 0.15wt.%GNPs content, the mechanical strength sharply declined because of the agglomerations of nano-ZrO$_2$ and graphene. Compared to pure aluminum, hardness and compressive strength increased by ~ 150% and ~ 163%, respectively.

(2) From the wear test results, wear rate (0.0031 mm^3/(Nm) at a 5 N load), minimum mass loss (11 mg at a 5 N load), and the lowest coefficient of friction (0.18 under a 10 N load) were determined Al-9ZrO$_2$-0.15GNPs composite. The increase in ZrO$_2$ and GNPs content improved the wear resistance up to 9wt.%ZrO$_2$ and 0.15wt.%GNPs content. In the case of over these contents, the wear resistance decreased due to the clustered nanoparticles. Besides, an increase in applied load caused a decrease in the friction coefficient and a rise in the wear rate. A decline in the coefficient of friction led to an improvement in contact load. This situation is caused by the intensity of the contact pressure, which may be enormous.

(3) XRD analyses revealed that the peak of graphene was not detected in any prepared composite because of too low graphene amount. Also, any in situ reactions and secondary phase formation were not observed in any ZrO$_2$-graphene reinforced Al composite. The secondary phase reactions occurred above the temperature of 950 °C, which might unfavorably affect the mechanical strength of Al-ZrO$_2$-GNPs composites. Hence, any secondary phase reactions were not observed due to the low sintering temperature (630 °C) in this study.

(4) SEM analyses showed good neck formation and a strong interface between particles. Also, the presence of ZrO$_2$ and graphene nanoparticles at the aluminum grain boundary was observed from the fracture surface of the SEM investigations. The worn surface morphologies showed the grooves' width and the damage on the surface, which decreased with increase in ZrO$_2$ and graphene amount up to 9%ZrO$_2$ and 0.15%GNPs. In the case of over these reinforcement rates, wear scars on the surface increased due to the clustered nanoparticles. As a result of the SEM image for the worn surfaces, the abrasive wear mechanism may be described as the main wear mechanism.

(5) In conclusion, zirconium dioxide is an effective ceramic material up to a specific ZrO$_2$ nanoparticle amount to decrease the material loss in the Al matrix. Also, graphene is an effective solid lubricator up to a certain GNPs content (0.15wt.%) to increase the wear resistance and load-bearing capacity.

Declarations

Conflict of interest The authors declared no potential conflicts of interest with respect to the research, authorship, and/or publication of this article.

References

1. Dieter, G.E.: Mechanical Metallurgy. McGraw-Hill, London (1961)
2. Song, W.; Veca, L.M.; Anderson, A.; Cao, M.; Cao, L.; Sun, Y.: Light-weight nanocomposite materials with enhanced thermal transport properties. Nanotechnol. Rev. **1**(4), 363–376 (2012). https://doi.org/10.1515/ntrev-2012-0023
3. Khan, A.; Matli, P.R.; Nawaz, M.; Mattli, M.R.: Microstructure and mechanical behavior of hot extruded aluminum/tin-bismuth composites produced by powder metallurgy. Appl. Sci. **10**(8), 1–14 (2020). https://doi.org/10.3390/app10082812
4. Reddy, M.; Khan, A.; Reddy, P.; Yusuf, M.; Ashraf, A.A.; Shakoor, R.A.: Gupta, M: Effect of Inconel625 particles on the microstructural, mechanical, and thermal properties of Al-Inconel625 composites. Mater. Today Commun. **25**, 1–12 (2020). https://doi.org/10.1016/j.mtcomm.2020.101564
5. Sharma, P.; Sharma, S.; Kandhuja, D.: Production and some properties of Si$_3$N$_4$ reinforced aluminium alloy. J. Asian. Ceram. Soc. **3**(3), 352–359 (2015). https://doi.org/10.1016/j.jascer.2015.07.002
6. Şenel, M.C.; Gürbüz, M.; Koç, E.: The fabrication and characterization of synergistic Al-SiC-GNPs hybrid composites. Compos. Part B Eng. **154**, 1–9 (2018). https://doi.org/10.1016/j.compositesb.2018.07.035
7. Khademian, M.; Alizadeh, A.; Abdollahi, A.: Fabrication and characterization of hot rolled and hot extruded boron carbide (B$_4$C) reinforced A356 aluminum alloy matrix composites produced by stir casting method. T. Indian I. Metals **70**(6), 1635–1646 (2017). https://doi.org/10.1007/s12666-016-0962-0
8. Gostariani, R.; Ebrahimi, R.; Asadabad, M.A.; Paydar, M.H.: Mechanical properties of Al/BN nanocomposites fabricated by planetary ball milling and conventional hot extrusion. Acta Metall. Sin. **31**, 245–253 (2018). https://doi.org/10.1007/s40195-017-0640-1
9. Şenel, M.C.; Gürbüz, M.: Investigation on mechanical properties and microstructures of aluminum hybrid composites reinforced with Al$_2$O$_3$/GNPs binary particles. Arch. Metall. Mater. **66**(1), 97–106 (2021). https://doi.org/10.24425/amm.2021.134764

10. Samal, P.; Vundavilli, P.R.; Meher, A.; Mahapatra, M.M.: Fabrication and mechanical properties of titanium carbide reinforced aluminium composites. Mater. Today. Proc. **18**(7), 2649–2655 (2019). https://doi.org/10.1016/j.matpr.2019.07.125

11. Suresh, S.; Shenbag, N.; Moorhi, V.: Aluminium-titanium diboride (Al-TiB$_2$) metal matrix composites: challenges and opportunities. Procedia Eng. **38**, 89–97 (2012). https://doi.org/10.1016/j.proeng.2012.06.013

12. Khan, A.; Abdelrazeq, M.W.; Mattli, M.R.; Yusuf, M.M.; Alashraf, A.; Matli, P.R.; Shakoor, R.A.: Structural and mechanical properties of Al-SiC-ZrO$_2$ nanocomposites fabricated by microwave sintering technique. Curr. Comput. Aid. Drug Des. **10**(10), 1–12 (2020). https://doi.org/10.3390/cryst10100904

13. Ravichandran, M.; Naveen Sait, A.; Anandakrishnan, V.: Al–TiO$_2$–Gr powder metallurgy hybrid composites with cold upset forging. Rare Met. **33**(6), 686–696 (2014). https://doi.org/10.1007/s12598-014-0239-x

14. Elango, G.; Raghunath, B.K.: Tribological behavior of hybrid (LM25Al + SiC+ TiO$_2$) metal matrix composites. Procedia Eng. **64**, 671–680 (2013). https://doi.org/10.1016/j.proeng.2013.09.142

15. El Mahallawi, I.; Shash, Y.; Rashad, R.M.; Abdelaziz, M.H.; Mayer, J.; Schwedt, A.: Hardness and wear behaviour of semi-solid cast A390 alloy reinforced with Al$_2$O$_3$ and TiO$_2$ nanoparticles. Arab. J. Sci. Eng. **39**, 5171–5184 (2014). https://doi.org/10.1007/s13369-014-1179-3

16. Mohapatra, S.; Mishra, D.K.; Mishra, G.; Roy, G.S.; Behera, D.; Mantry, S.; Singh, S.K.: A study on sintered TiO$_2$ and TiO$_2$/SiC composites synthesized through chemical reaction based solution method. J. Compos. Mater. **47**(24), 3081–3089 (2013). https://doi.org/10.1177/0021998312462430

17. Muley, A.V.; Aravindan, S.; Singh, I.P.: Nano and hybrid aluminum based metal matrix composites: an overview. Manuf. Rev. **2**(15), 1–13 (2015). https://doi.org/10.1051/mfreview/2015018

18. Bodunrin, M.O.; Alaneme, K.K.; Chown, L.H.: Aluminium matrix hybrid composites: A review of reinforcement philosophies; mechanical, corrosion and tribological characteristics. J. Mater. Res. Technol. **4**(4), 434–445 (2015). https://doi.org/10.1016/j.jmrt.2015.05.003

19. Madhukar, P.; Selvaraj, N.; Rao, C.S.P.: Manufacturing of aluminium nano hybrid composites: a state of review. IOP Conf. Ser. Mater. Sci. Eng. **149**(012114), 1–12 (2016). https://doi.org/10.1088/1757-899X/149/1/012114

20. Iacob, G.; Ghica, V.G.; Buzatu, M.; Buzatu, T.; Petrescu, M.I.: Studies on wear rate and micro-hardness of the Al/Al$_2$O$_3$/Gr hybrid composites produced via powder metallurgy. Compos. Part B Eng. **69**, 603–611 (2015). https://doi.org/10.1016/j.compositesb.2014.07.008

21. Alizadeh, A.; Abdollahi, A.; Biukani, H.: Creep behavior and wear resistance of Al 5083 based hybrid composites reinforced with carbon nanotubes (CNTs) and boron carbide (B$_4$C). J. Alloys. Compd. **650**, 783–793 (2015). https://doi.org/10.1016/j.jallcom.2015.07.214

22. Zhang, X.N.; Geng, L.; Wang, G.S.: Fabrication of Al-based hybrid composites reinforced with SiC whiskers and SiC nanoparticles by squeeze casting. J. Mater. Process. Technol. **176**(1–3), 146–151 (2006). https://doi.org/10.1016/j.jmatprotec.2006.03.125

23. Geim, A.K.; Novoselov, K.S.: The rise of graphene. Nat. Mater. **6**, 183–191 (2007). https://doi.org/10.1038/nmat1849

24. Savage, N.: Materials science: super carbon. Nature **483**, 30–31 (2012). https://doi.org/10.1038/483S30a

25. Singh, V.; Joung, D.; Zhai, L.; Das, S.; Khondaker, S.I.; Seal, S.: Graphene based materials: past, present and future. Prog. Mater. Sci. **56**(8), 1178–1271 (2012). https://doi.org/10.1016/j.pmatsci.2011.03.003

26. Berman, D.; Erdemir, A.; Sumant, A.V.: Graphene: a new emerging lubricant. Mater. Today **17**(1), 31–42 (2014). https://doi.org/10.1016/j.mattod.2013.12.003

27. Udayashankar, S.; Ramamurthy, V.S.: Development and characterization of Al6061-zirconium dioxide reinforced particulate composites. Int. J. Eng. Technol. **7**(3.12), 128–132 (2018). https://doi.org/10.14419/ijet.v7i3.12.15901

28. Kumar, H.G.P.; Xavior, M.A.: Effect of graphene addition on flexural properties of Al6061 nano composites. Mater. Today. Proc. **4**(8), 8127–8133 (2017). https://doi.org/10.1016/j.matpr.2017.07.153

29. Boppana, S.B.; Dayanand, S.; Kumar, A.; Kumar, V.; Aravinda, T.: Synthesis and characterization of nano graphene and ZrO$_2$ reinforced Al 6061 metal matrix composites. J. Mater. Res. Tech. **9**(4), 7354–7362 (2020). https://doi.org/10.1016/j.jmrt.2020.05.013

30. Chen, L.; Qi, Y.; Fei, Y.; Du, Z.: Enhanced mechanical properties and thermal conductivity for GNPs/Al2024 composites with in situ SiC nanorods. Met. Mater. Int. (2021). https://doi.org/10.1007/s12540-020-00803-9

31. AbuShanab, W.S.; Moustafa, E.B.; Ghandourah, E.; Taha, M.A.: Effect of graphene nanoparticles on the physical and mechanical properties of the Al2024-graphene nanocomposites fabricated by powder metallurgy. Results Phys. **19**, 1–12 (2020). https://doi.org/10.1016/j.rinp.2020.103343

32. Shin, S.E.; Ko, Y.J.; Bae, D.H.: Mechanical and thermal properties of nanocarbon-reinforced aluminum matrix composites at elevated temperatures. Compos. Part B Eng. **106**, 66–73 (2016). https://doi.org/10.1016/j.compositesb.2016.09.017

33. Zheng, Z.; Yang, X.; Li, J.C.; Zhang, X.X.; Muhammad, I.; Geng, L.: Preparation and properties of graphene nanoplatelets reinforced aluminum composites. Trans. Nonferrous Met. Soc. China **31**(4), 878–886 (2021). https://doi.org/10.1016/S1003-6326(21)65546-2

34. Chak, V.; Chattopadhyay, H.: Fabrication and heat treatment of graphene nanoplatelets reinforced aluminium nanocomposites. Mat. Sci. Eng. A Struct. **791**, 1–10 (2021). https://doi.org/10.1016/j.msea.2020.139657

35. Yu, H.; Zhang, S.Q.; Xia, J.H.; Su, Q.; Ma, B.C.; Wu, J.H.; Zhou, J.X.; Wang, X.T.; Hu, L.X.: Microstructural evolution, mechanical and physical properties of graphene reinforced aluminum composites fabricated via powder metallurgy. Mat. Sci. Eng. A Struct. **802**, 1–10 (2021). https://doi.org/10.1016/j.msea.2020.140669

36. Kumar, H.G.P.; Xavior, M.A.: Assessment of mechanical and tribological properties of Al 2024-SiC-Graphene hybrid composites. Procedia Eng. **174**, 992–999 (2017). https://doi.org/10.1016/j.proeng.2017.01.251

37. Şenel, M.C.; Gürbüz, M.; Koç, E.: Mechanical and tribological behaviours of aluminium matrix composites reinforced by graphene nanoplatelets. Mater. Sci. Tech. Lond. **34**(16), 1980–1989 (2018). https://doi.org/10.1080/02670836.2018.1501839

38. Gürbüz, M.; Şenel, M.C.: Koç, E: The effect of sintering temperature, time and graphene addition on the mechanical properties and microstructure of aluminum composites. J. Compos. Mater. **52**(4), 553–563 (2018). https://doi.org/10.1177/0021998317740200

39. Şenel, M.C.; Gürbüz, M.; Koç, E.: The fabrication and characterization of aluminum hybrid composites reinforced with silicon nitride/graphene nanoplatelet binary particles. J. Compos. Mater. **53**, 4043–4054 (2019). https://doi.org/10.1177/0021998319853329

40. Pandiyarajan, R.; Maran, P.; Marimuthu, S.; Ganesh, K.C.: Mechanical and tribological behavior of the metal matrix composite AA6061/ZrO$_2$/C. J. Mech. Sci. Technol. **31**(10), 4711–4717 (2017). https://doi.org/10.1007/s12206-017-0917-3

41. Kumar, G.B.V.; Pramod, R.; Sekhar, C.G.; Kumar, G.P.; Bhanumurthy, T.: Investigation of physical, mechanical and tribological properties of Al6061-ZrO$_2$ nano-composites. Heliyon **5**(11), 1–8 (2019). https://doi.org/10.1016/j.heliyon.2019.e02858

42. Abdizadeh, H.; Baghchesara, M.A.: Investigation on mechanical properties and fracture behavior of A356 aluminum alloy based ZrO_2 particle reinforced metal-matrix composites. Ceram. Int. **39**(2), 2045–2050 (2013). https://doi.org/10.1016/j.ceramint.2012.08.057

43. Salimi, A.; Borhani, E.; Emadoddin, E.: Evaluation of mechanical properties and structure of 1100-Al reinforced with ZrO_2 nanoparticles via accumulatively roll-bonded. Proc. Mat. Sci. **11**, 67–73 (2015). https://doi.org/10.1016/j.mspro.2015.11.094

44. Hemanth, J.: Development and property evaluation of aluminum alloy reinforced with nano-ZrO_2 metal matrix composites (NMMCs). Mater. Sci. Eng. A Struct. **507**(1–2), 110–113 (2009). https://doi.org/10.1016/j.msea.2008.11.039

45. Madhusudhan, M.; Naveen, G.J.; Mahesha, K.: Mechanical characterization of AA7068-ZrO_2 reinforced metal matrix composites. Mater. Today Proc. **4**(2), 3122–3130 (2017). https://doi.org/10.1016/j.matpr.2017.02.196

46. Ramachandra, M.; Abhishek, A.; Siddeshwar, P.; Bharathi, V.: Hardness and wear resistance of ZrO_2 nano particle reinforced Al nanocomposites produced by powder metallurgy. Proc. Mater. Sci. **10**, 212–219 (2015). https://doi.org/10.1016/j.mspro.2015.06.043

47. Zhai, W.; Shi, X.; Yao, J.; Ibrahim, A.M.M.; Xiu, Z.; Zhu, Q.; Xiao, Y.; Chen, L.; Zhang, Q.: Investigation of mechanical and tribological behaviors of multilayer graphene reinforced Ni_3Al matrix composites. Compos. Part B Eng. **70**, 149–155 (2015). https://doi.org/10.1016/j.compositesb.2014.10.052

48. Liu, R.; Li, D.Y.: Modification of Archard's equation by taking account of elastic/ pseudoelastic properties of materials. Wear **251**(1–12), 956–964 (2001). https://doi.org/10.1016/S0043-1648(01)00711-6

49. Kaczmar, J.W.; Pietrzak, K.; Wlosinski, W.: The production and application of metal matrix composite materials. J. Mater. Process. Tech. **106**(1–3), 58–67 (2000). https://doi.org/10.1016/S0924-0136(00)00639-7

50. Li, G.; Xiong, B.: Effects of graphene content on microstructures and tensile property of graphene-nanosheets/aluminum composites. J. Alloy. Compd. **697**, 31–36 (2017). https://doi.org/10.1016/j.jallcom.2016.12.147

51. Habibi, M.K.; Joshi, S.P.; Gupta, M.: Hierarchical magnesium nano-composites for enhanced mechanical response. Acta Mater. **58**(18), 6104–6114 (2010). https://doi.org/10.1016/j.actamat.2010.07.028

52. Hu, Z.; Tong, G.; Nian, Q.; Xu, R.; Saei, M.; Chen, F.; Chen, C.; Zhang, M.; Guo, H.; Xu, J.: Laser sintered single layer graphene oxide reinforced titanium matrix nanocomposites. Compos. Part B Eng. **93**, 352–359 (2016). https://doi.org/10.1016/j.compositesb.2016.03.043

53. Cao, Z.; Wang, X.; Li, J.; Wu, Y.; Zhang, H.; Guo, J.; Wang, S.: Reinforcement with graphene nanoflakes in titanium matrix composites. J. Alloy. Compd. **696**, 498–502 (2017). https://doi.org/10.1016/j.jallcom.2016.11.302

54. Torralba, J.M.; Costa, C.E.; Velasco, F.: P/M aluminum matrix composites: an overview. J. Mater. Process. Tech. **133**(1–2), 203–206 (2003). https://doi.org/10.1016/S0924-0136(02)00234-0

55. Chen, L.Y.; Konishi, H.; Fehrenbacher, A.; Ma, C.; Xu, J.Q.; Choi, H.; Xu, H.F.; Pfefferkorn, F.E.; Li, X.C.: Novel nanoprocessing route for bulk graphene nanoplatelets reinforced metal matrix nanocomposites. Scripta Mater. **67**(1), 29–32 (2012). https://doi.org/10.1016/j.scriptamat.2012.03.013

56. Wang, J.; Li, Z.; Fan, G.; Pan, H.; Chen, Z.; Zhang, D.: Reinforcement with graphene nanosheets in aluminum matrix composites. Scripta Mater. **66**, 594–597 (2012). https://doi.org/10.1016/j.scriptamat.2012.01.012

57. Wang, Z.; Georgarakis, K.; Zhang, W.W.; Prashanth, K.G.; Eckert, J.; Scudino, S.: Reciprocating sliding wear behavior of high-strength nanocrystalline $Al_{84}Ni_7Gd_6Co_3$ alloys. Wear **382–383**, 78–84 (2017). https://doi.org/10.1016/j.wear.2017.04.013

58. Rajeev, V.R.; Dwivedi, D.K.; Jain, S.C.: Dry reciprocating wear of Al–Si–SiCp composites: a statistical analysis. Tribol. Int. **43**(8), 1532–1541 (2010). https://doi.org/10.1016/j.triboint.2010.02.014

59. Liu, Y.; Han, Z.; Cong, H.: Effects of sliding velocity and normal load on the tribological behavior of a nanocrystalline Al based composite. Wear **268**(7–8), 976–983 (2010). https://doi.org/10.1016/j.wear.2009.12.027

60. Kumar, N.M.; Kumaran, S.S.; Kumaraswamidhas, L.A.: Wear behaviour of Al 2618 alloy reinforced with Si_3N_4, AlN and ZrB_2 in situ composites at elevated temperatures. Alex. Eng. J. **55**(1), 19–36 (2016). https://doi.org/10.1016/j.aej.2016.01.017

61. Kumar, H.G.P.; Xavior, M.A.: Fatigue and wear behavior of Al6061–graphene composites synthesized by powder metallurgy. T. Indian I. Metals **69**(2), 415–419 (2016). https://doi.org/10.1007/s12666-015-0780-9